Shielded-Capacitive Power Transfer for EVs : Matching and Peak Width Improvement

Naoki KOJO[1] Kosei KAMZUKA[1] Hao CHEN[2] Haruichi KANAYA[2]
Eiichi TATEISHI[3] Nobuhiro KAI[3] Toru HASHIMOTO[3] Kota UCHIO[3]
Yuta IDE[3] Tatsuya YAMAGUCHI[4] Hussein MAHDI[5] and Reiji HATTORI[1]

[1]Interdisciplinary Graduate School of Engineering Sciences, Kyushu University, Fukuoka, 816-8580, Japan
[2]Graduate School of ISEE, Kyushu University, Fukuoka, 819-0395, Japan
[3]HINODE Holdings Co, Ltd, Fukuoka, 812-8636, Japan
[4]HINODE, Ltd, Fukuoka, 812-8636, Japan
[5]Department of Electrical Engineering, UiT-The Arctic University of Norway, Narvik 8514, Norway
E-mail: [1]hattori.reiji.082@m.kyushu-u.ac.jp, [2]kanaya@ed.kyushu-u.ac.jp
[3]e-tateishi@hinodesuido.co.jp, [4]t-yamaguchi@hinodesuido.co.jp, [5]hussein.al-sallami@uit.no

Abstract A circuit configuration that increases the peak width in the power transmission characteristic spectrum is examined to construct a robust system against circuit constant fluctuations by external disturbance in a capacitive power transfer (CPT) circuit aimed at wireless power supply to EVs and confirmed this through experiments and circuit simulations. By examining matching conditions and controlling the peak width, a power transfer efficiency of 80% was achieved at a transmission power of 300 W with an electrode gap of 10 cm.

Keywords CPT, EVs, Peak Width

1. Introduction

In recent years, there has been growing interest in EVs as part of efforts to achieve carbon neutrality. However, compared to gasoline-powered vehicles, EVs face several challenges: (1) shorter driving range per full charge, (2) longer charging times, and (3) the need for large-capacity batteries to enable long-distance travel, which ultimately increases the overall vehicle cost. As a result, the widespread adoption of EVs has yet to be fully realized [1].

One potential solution to these challenges is wireless power transfer (WPT). In particular, dynamic wireless power transfer (DWPT) [2-4], which allows charging while driving, has the potential to overcome the aforementioned issues. Thus, the advancement of WPT technology is considered a crucial factor in promoting the adoption of EVs [5].

WPT systems are mainly classified into two types: inductive power transfer (IPT) and capacitive power transfer (CPT). While IPT enables relatively long-distance power transmission [6], it is sensitive to misalignment. Additionally, IPT requires ferrite materials to increase magnetic flux density, and Litz wire for the transmission and receiving coils when operating at high frequencies for system miniaturization. These materials are heavy and expensive, leading to increased system cost and weight.

On the other hand, although CPT has a shorter transmission distance, it is more tolerant to misalignment. Moreover, CPT systems can use relatively lightweight and cost-effective materials such as aluminum for the transmitting and receiving electrodes, enabling system weight reduction and cost savings [7]. If sufficient capacitance can be secured, CPT also offers high design flexibility due to the freedom in electrode shape. These features suggest that CPT is more suitable as a wireless power transfer method for electric vehicles.

In wireless power transmission systems, various factors such as load fluctuations, positional shifts of coupling electrodes and their distance variations can cause the breakdown of impedance matching conditions, potentially reducing power transmission efficiency. Therefore, it is important to maintain matching conditions through closed-loop control. In this case, the width of the peak obtained from the power transmission characteristic spectrum is an important parameter that determines control stability and efficiency. In other words, a wider peak width results in a more gradual change in transmitted power and efficiency in response to slight variations in circuit constants. This allows the control system to tolerate some fluctuations, enabling a robust design. Additionally, since strict frequency tracking is not required, control becomes easier, resulting in faster overall system response.

In this paper, we have examined a circuit configuration that increases the peak width in the power transmission characteristic spectrum to construct a robust system against circuit constant fluctuations by external disturbance in CPT system aimed at wireless power supply to EVs and confirmed this through experiments and circuit simulations.

2. S-CPT SYSTEM

Simple CPT transmits power via an electric field formed between a pair of facing transmitting and receiving electrodes. However, since CPT relies on electric fields, it tends to leak electric fields outside the system, which may adversely affect nearby humans or electronic devices.

To address these issues, we have been researching the shielded capacitive power transfer (S-CPT) system which incorporates shield electrodes on the outer side of the transmitting and receiving electrodes [8-12]. Fig. 1 illustrates the S-CPT system as applied to EV charging.

The S-CPT system consists of three parts: the primary side, the power transmission/reception section, and the secondary side. High-frequency, high-voltage AC power generated on the primary side is transferred from the transmitting to the receiving electrodes through the electric field. On the secondary side, this power is converted into DC by a rectifier. Then, a DC-DC converter adjusts the voltage level to suit battery charging.

S-CPT systems, a typical configuration is the 6-plate structure, which uses two pairs of electrodes to form two capacitors. However, this study adopts a 4-plate structure. By dividing the shield electrodes in half and forming a half-circuit configuration, the system can also be applied to a 6-plate structure. The next chapter will provide a detailed explanation of this study based on the 4-plate configuration.

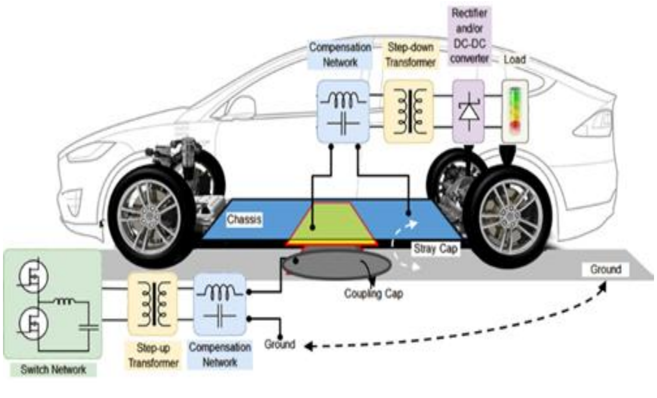

Fig. 1 Charging electric vehicles using S-CPT

3. DESIGN OF 4-PLATE

3.1. CALCULATING MATCHING CONDITIONS

In this study, the distance between the electrodes was fixed at 10 cm during the experiment. This distance complies with Z1 of the standards specified by SAE [13]. A high-frequency power supply with a frequency of 13.56 MHz was used as the power source. At this frequency, the coupling capacitance C_c formed between the transmitting and receiving electrodes is 12 pF, the shielding capacitance C_1 between the transmitting electrode and the shielding electrode is 36 pF, and the shielding capacitance C_2 between the receiving electrode and the shielding electrode is 32 pF.

The equivalent circuit of the S-CPT is shown in Fig. 2. Here, V_i represents the AC power source, R_L is the load resistance, and L is the inductance of the coil. The value of R_L is 50 Ω, which corresponds to the termination resistance of the oscilloscope.

In this study, the derivation of the matching condition follows the method described in [9]. However, while [8] assumes $C_2 = C_1$, in this study we set $C_2 = bC_1$, $b = 8/9$ for the derivation. The circuit equation derived by applying Kirchhoff's law to the equivalent circuit shown in Fig. 2 is given in (1), where ω denotes the angular frequency. By solving (1), the total impedance of the circuit, Z_{total} is expressed as (2). For impedance matching, the total impedance must satisfy $Z_{total} = 50 + j0$. From the condition that the imaginary part becomes zero, the inductance L can be determined, which is expressed in (3). The parameter D_1 in (3) is defined by (4). Furthermore, by substituting (3) into (2), the real part of Z_{total}, namely the resistive component Z_{real}, can be obtained, as shown in (5).

Using (5), a graph is plotted in Fig. 3 with the load resistance R_L on the horizontal axis and the real part of the impedance Z_{real} on the vertical axis. This graph shows the relationship between Z_{real} and R_L when the coupling capacitance C_c is varied (5 pF, 12 pF, 30 pF, and 50 pF), while C_1 and C_2 are fixed at 36 pF and 32 pF, respectively. In this study, C_c is set to 12 pF and the load resistance to 50 Ω. Therefore, the corresponding point is indicated by a red circle in the graph. At this point, the value of Z_{real} is 3.03 Ω, which does not match 50 Ω, as can be confirmed from the graph.

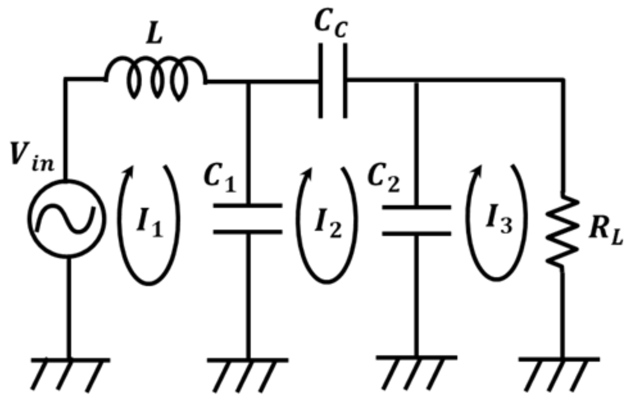

Fig. 2 Equivalent Circuit of the S-CPT

$$\begin{bmatrix} j\omega L_1 + \frac{1}{j\omega C_1} & -\frac{1}{j\omega C_1} & 0 \\ -\frac{1}{j\omega C_1} & \frac{1}{j\omega C_1} + \frac{1}{j\omega C_2} + \frac{1}{j\omega C_c} & -\frac{1}{j\omega C_2} \\ 0 & -\frac{1}{j\omega C_2} & \frac{1}{j\omega C_2} + R_L \end{bmatrix} \begin{bmatrix} I_1 \\ I_2 \\ I_3 \end{bmatrix} = \begin{bmatrix} V_{in} \\ 0 \\ 0 \end{bmatrix} \tag{1}$$

$$Z_{total} = -\omega^3 C_1 R_L L_1 (bC_1 + bC_c + C_c) + i\omega^2 L_1 (C_1 + C_c) + \omega R_L (bC_1 + C_c) - i\,/\omega\{(C_1 + C_c) - i\omega C_1 R_L (bC_1 + bC_c + C_c)\} \tag{2}$$

$$L = \omega^2 R_L^2 (b^2 C_1^3 + b^2 C_1^2 C_c + 2bC_1^2 C_c + bC_1 C_c^2 + C_1 C_c^2) + (C_1 + C_C)/D_1 \tag{3}$$

$$D_1 = \omega^4 R_L^2 (b^2 C_1^4 + 2b^2 C_1^3 C_c + 2bC_1^3 C_c + b^2 C_1^2 C_c^2 + 2bC_1^2 C_c^2 L + C_1^2 C_c^2) + \omega^2 (C_1 + C_c)^2 \tag{4}$$

$$Z_{real} = \frac{C_c^2 R_L}{D_1} \tag{5}$$

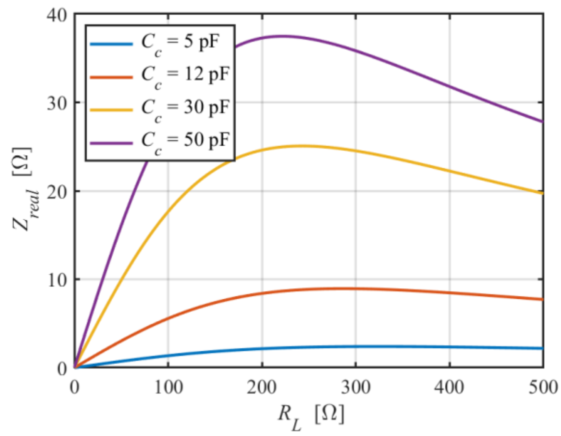

Fig. 3 Real Part of impedance vs. Load Resistance

As shown in Fig. 4, an L-type matching network was added. In general, when the load resistance on the output side is smaller than the resistance on the input side, impedance matching can be achieved by inserting an L-type network as in Fig. 4. In this study, adding the L-type matching network results in two coils; however, since they are connected in series, they can be treated as a single equivalent coil. Moreover, because this study employs variable capacitors C_{tune} and C_{Load}, the configuration can be represented, as in Fig. 5, by a variable coil L_1 and variable capacitor C_{Load}.The parameters of L_1 and C_{Load} were then adjusted to achieve impedance matching.

Fig. 6(a) shows the measurement results on the Smith chart. The measurement frequency range was 10 MHz to 20 MHz, and the red marker indicates the measured point at 13.56 MHz. At this frequency, Z_{total} was 49.93+j(−0.39) Ω. The LTspice simulation results are shown in Figure 6(b), where it can be seen that the same trend as in the experimental results was obtained.

Fig. 7 shows the return loss of S_{11}, indicating a value of -48.08 dB at 13.56 MHz. From these results, it is confirmed that the circuit is in a resonant state at 13.56 MHz, that reflections are reduced, and that impedance matching with 50 Ω is achieved.

On the other hand, as is evident from Fig. 7, the circuit exhibits high resonance sharpness and a very narrow peak width. As a result, even slight variations in component parameters can cause significant changes in impedance, potentially breaking the matching condition. In particular, since an automatic matching device is used in this study, it becomes difficult to track such rapid impedance changes. Therefore, in the next section, a method to broaden the peak width is investigated.

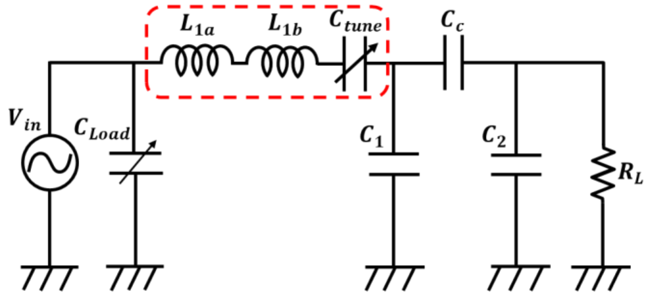

Fig. 4 S-CPT Circuit with Added L-Network

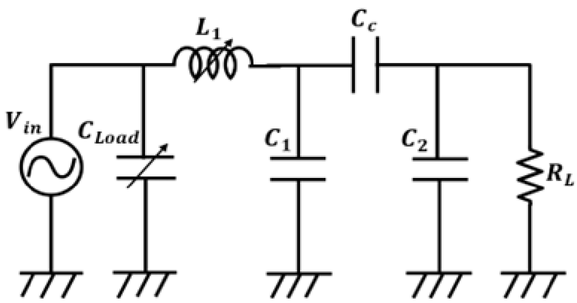

Fig. 5 Simplified circuit

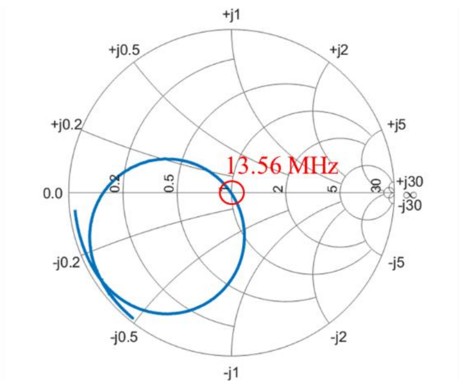

(a) Experiment

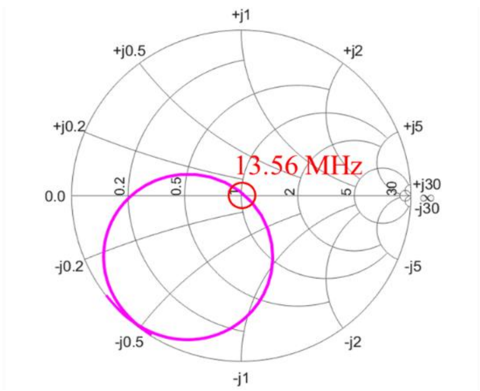

(b) Simulation
Fig. 6 Smith Chart

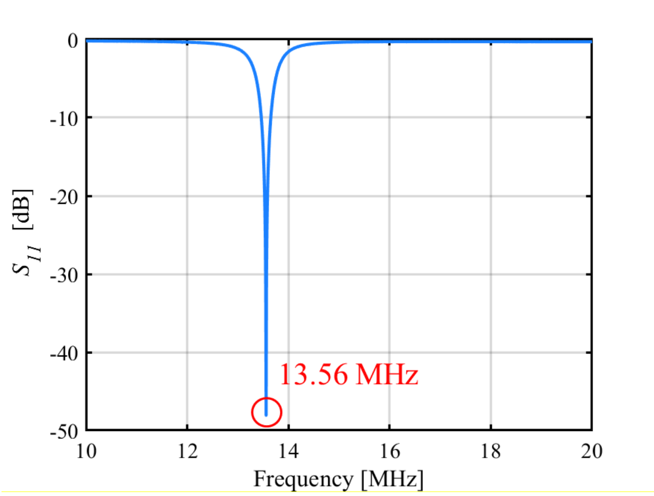

Fig. 7 S_{11} vs. Frequency

3.2. PEAK WIDTH IMPROVEMENT

To determine the resonance sharpness of the circuit in Fig. 5, the inductance L_1 is divided into two parts, L_{1a} and L_{1b}, as shown in Fig. 8, and the circuit on the load side from L_{1b} is denoted as R_L'. The Q value, which represents the resonance sharpness, is given by (6). Here, R_0 is the characteristic impedance of the coaxial cable (50 Ω). A larger Q value indicates sharper resonance and a narrower peak width, while a smaller Q value indicates gentler resonance and a wider peak width. For the actual value of this circuit, the results in Fig. 1 show that R_L'=3.03 Ω. This confirms, from a theoretical standpoint, that the circuit in Fig. 5 has a very narrow peak width. Furthermore, Fig. 1 shows that decreasing C_c reduces R_L', thereby increasing the Q value. Considering future applications in which the electrode gap is increased for power transfer, it is necessary to broaden the peak width.

Therefore, the circuit was also evaluated for the case in which an inductor L_2 was inserted on the load side. As shown in Fig. 9, the inductance L_1 was divided into two parts, L_{1a} and L_{1b}, and the circuit on the load side from L_{1b} was denoted as R_L'. For the circuit represented by R_L', Kirchhoff's law was applied in the same manner as described in Section 3.1, and the condition in which the imaginary part of the impedance becomes zero was determined, yielding (7). The parameter D_2 in (7) is defined in (8).

Using (7), a graph was plotted in Fig. 10 with the load resistance R_L on the horizontal axis and R_L' on the vertical axis. From this graph, it can be observed that increasing the value of L_2 increases R_L', thereby reducing the Q value and, as a result, broadening the peak width.

Figure 11(a) shows the experimental results before and after inserting coil L_2. The results confirm that the insertion L_2 broadens the peak width and improves the responsiveness to impedance variations. A similar tendency was also observed in the simulation, as shown in Fig. 11(b). Based on these findings, the circuit shown in the figure was adopted for the power transmission experiments in this study.

$$Q = \sqrt{\frac{R_0}{R_L'} - 1} \tag{6}$$

$$R_L' = \frac{C_c^2 R_L}{D_2} \tag{7}$$

$$D_2 = \omega^4 C_1^2 L_2^2 (C_1 b + C_c b + C_c)^2 + \omega^2 C_1 (C_1 b + C_c b + C_c)(C_1^2 R_L^2 b + C_1 C_c R_L^2 b + C_1 C_c R_L^2 - 2C_1 L_2 - 2C_c L_2) + (C_1 + C_c)^2 \tag{8}$$

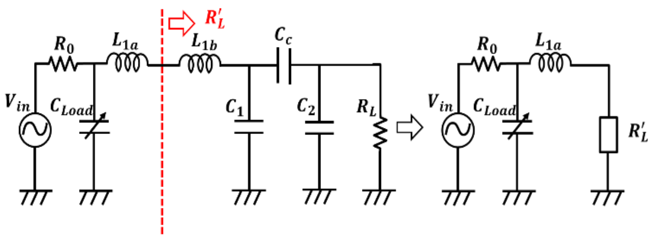

Fig. 8 Simplified Circuit for Q-Factor Calculation

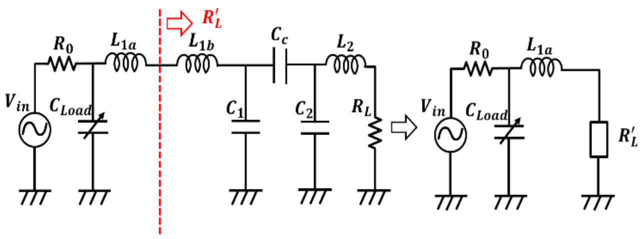

Fig. 9 Equivalent Circuit with L_2 for Q-Factor Calculation

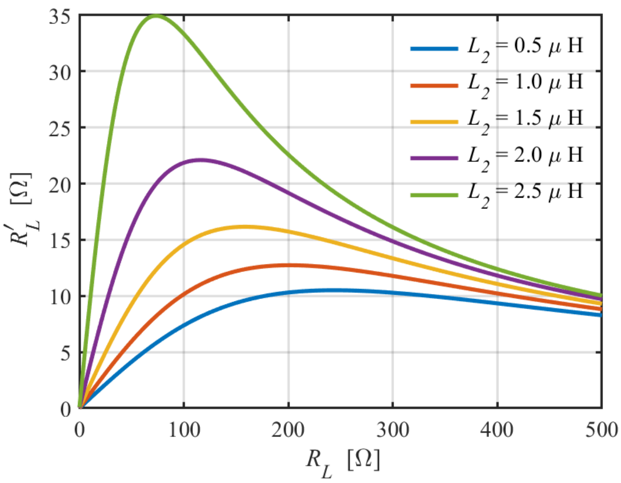

Fig. 10 Real Part of Impedance vs. Load Resistance

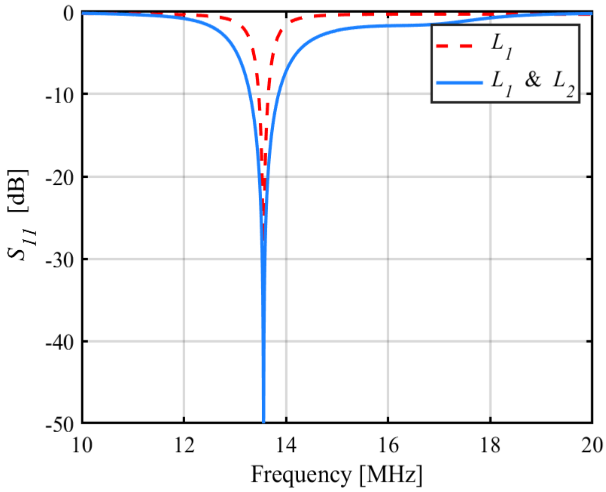

(a) Experiment

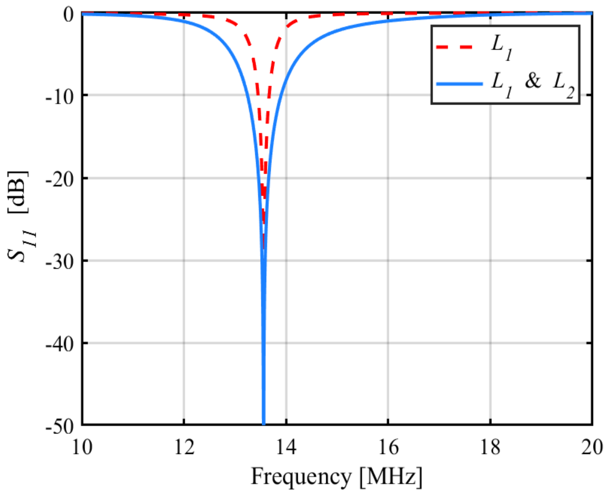

(b) Simulation

Fig. 11 S_{11} vs. Frequency

3.3. Power transmission experiment

The power transmission test was conducted using a circuit with L_2 inserted on the load side. The experiment setup is shown in Fig. 12. In this study, the voltage V_{out} across the load R_L was measured using an oscilloscope while the power was attenuated by 30 dB with an attenuator, and the output power P_{out} was calculated using equation (9). Furthermore, the power transmission efficiency η was determined using equation (10). The results are shown in Fig. 13. As can be seen from the figure, the power transmission efficiency exceeded 80%. The difference from 100% can be attributed to factors such as heat losses in L_1 and L_2, as well as electric field leakage to the surroundings.

$$P_{out} = \frac{{V_{out}}^2}{R_L} \times 1000 \ \text{[W]} \tag{9}$$

$$\eta = \frac{P_{out}}{P_{in}} \times 100 \ [\%] \tag{10}$$

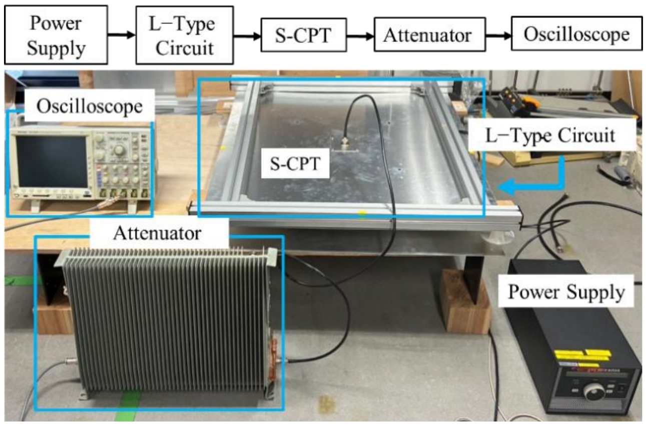

Fig. 12 Circuit for Power Transmission Experiment

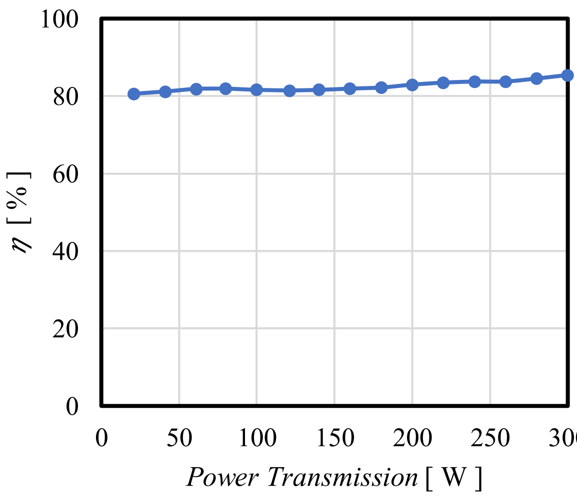

Fig. 13 Power Transmission Test Results up to 300W

4. Conclusion

We focused on charging electric vehicles using shielded capacitive wireless power transfer. By setting the matching conditions and improving the peak width, we achieved a power transfer efficiency of over 80% at a transmission power of 300 W with an electrode gap of 10 cm. In future work, we plan to apply this approach to the 6-plate configuration and investigate a rectifier for converting AC to DC, as well as a DC-DC converter for controlling the output voltage.

References

[1] Zhao, Wei, and Asako Terasawa. "A Study on Future Trends of Electric Vehicles." *Bulletin of the Institute of Industrial and Economic Research* 25 (2015): 211–227.

[2] Kim, J.; Bien, F. Electric field coupling technique of wireless power transfer for electric vehicles. In Proceedings of the IEEE 2013 Tencon-Spring Conference, Sydney, Australia, 17–19 April 2013; pp. 267–271.

[3] Sakai, N.; Itokazu, D.; Suzuki, Y.; Sakihara, S.; Ohira, T. One-kilowatt capacitive power transfer via wheels of a compact electric vehicle. In Proceedings of the Wireless Power Transfer Conference, Aveiro, Portugal, 5–6 May 2016; pp. 1–3.

[4] Vu, V.; Kamal, L.; Tay, J.; Pickert, V.; Dahidah, M.; Logenthiran, T.; Phan, V. A multi-output capacitive charger for electric vehicles. In Proceedings of the 2017 IEEE 26th International Symposium on Industrial Electronics (ISIE), Edinburgh, UK, 19–21 June 2017; pp. 565–569.

[5] Takuma Ishibashi. "Farewell to EV Battery Depletion." *Nikkei Electronics*, November 2024, pp. 34–49.

[6] Dai, J.; Ludois, D.C. "A Survey of Wireless Power Transfer and a Critical Comparison of Inductive and Capacitive Coupling for Small Gap Applications." *IEEE Trans. Power Electron.* 2015, *30*, 6017–6029.

[7] Kenichi Harakawa, and Kazuyuki Miura, "Possibility of Wireless Power Supply by Electric Coupling Technology." *Takenaka Technical Research Report*, no. 66. 2020, 1–8.

[8] Ahmad, Suziana, Aam Muharam, Reiji Hattori, Anyu Uezu, and Tarek M. Mostafa, "Shielded Capacitive Power Transfer (S-CPT) without Secondary Side Inductors," Energies 14, no. 15: 4590, July, 2021.

[9] Suziana Ahmad, Reiji Hattori, Aam Muharam, An-yu Uezu, "Preliminary Design by Modeling S-CPT System With Inductance Consideration," 2021 IEEE PELS Workshop on Emerging Technologies: Wireless Power Transfer (WoW), 2021.

[10] Suziana Ahmad, Aam Muharam, Reiji Hattori, Anyu Uezu, Tarek M. Mostafa, "Shielded Capacitive Power Transfer (S-CPT) without Secondary Side Inductors," Energies 2021, 14(15), 4590, 2021.

[11] Suziana Ahmad, Reiji Hattori, Aam Muharam, "Generalized Circuit Model of Shielded Capacitive Power Transfer," Energies 2021, 14(10), 2826, 2021.

[12] Aam Muharam, Suziana Ahmad, Reiji Hattori, "Scaling-factor and Design Guidelines for Shielded-Capacitive Power Transfer," Energies, vol 13, Issue 6, p.4240, 2020.

[13] Dejana Herceg, Vladimir Rajs, Živadin Despotović, Bane Popadić, Mirjana Šiljegović, Zoltan Kiraly, Zoltan Vizvari, Krisztian Wizner, Imre Felde, Peter Odry, Vladimir Tadić, "Double-Layer Coils Design for 11 kW Wireless Power Transfer," Electronics, vol 13, Issue 3, p.547, 2024.